

ViewDelta: Text-Prompted Change Detection in Unaligned Images

Subin Varghese

University of Houston

4302 University Dr, Houston, TX 77004

srvargh2@cougarnet.uh.edu

Joshua Gao

University of Houston

4302 University Dr, Houston, TX 77004

jkgao@cougarnet.uh.edu

Vedhus Hoskere

University of Houston

4302 University Dr, Houston, TX 77004

vhoskere@central.uh.edu

Abstract

Detecting changes between images is fundamental in applications such as infrastructure assessment, environmental monitoring, and industrial automation. Existing supervised models demonstrate strong performance but are inherently limited by the scope of their training data, requiring retraining to recognize novel changes. To overcome this limitation, we introduce a novel change detection task utilizing textual prompts alongside two potentially unaligned images to produce binary segmentations highlighting user-relevant changes. This text-conditioned framework significantly broadens the scope of change detection, enabling unparalleled flexibility and straightforward scalability by incorporating diverse future datasets without restriction to specific change types. As a first approach to address this challenge, we propose ViewDelta, a multimodal architecture extending the vision transformer into the domain of text-conditioned change detection. ViewDelta establishes a robust baseline, demonstrating flexibility across various scenarios and achieving competitive results compared to specialized, fine-tuned models trained on aligned images. Moreover, we create and release the first text-prompt-conditioned change detection dataset, comprising 501,153 image pairs with corresponding textual prompts and annotated labels. Extensive experiments confirm the robustness and versatility of our model across diverse environments, including indoor, outdoor, street-level, synthetic, and satellite imagery. github.io/viewdelta/

1. Introduction

Detecting and understanding changes between images is a critical task in computer vision [3, 9, 20, 39], with applications spanning situational awareness [14, 47], infrastruc-

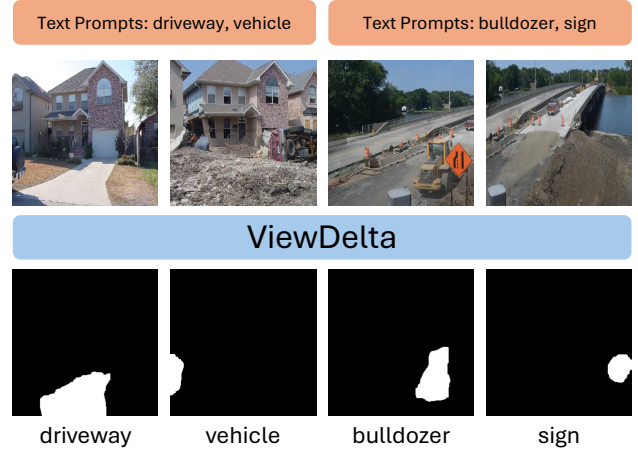


Figure 1. Given a pair of aligned or unaligned images captured before and after an event, alongside a textual prompt specifying user-relevant changes, ViewDelta outputs a segmentation highlighting the desired changes.

ture damage assessment [35, 38, 41, 45], and environmental monitoring [18, 28].

Traditional change detection methods typically require pairs of aligned images and focus on predefined types of changes, limiting their applicability to scenarios where alignment cannot be guaranteed or when encountering novel change types not represented during training. Such methods thus struggle in real-world settings, which often involve varying viewpoints or camera orientations, resulting in significant performance degradation.

To overcome these limitations, we introduce ViewDelta (see Fig. 1), a novel approach enabling robust, user-defined, prompt conditioned change detection for unaligned image pairs. By leveraging natural language prompts, ViewDelta

provides users the flexibility to specify desired changes explicitly, accommodating diverse applications within a single generalized model. Due to the added flexibility of a input prompt, our method can effectively handle images from a wide range of domains, such as street-level and satellite imagery, without the necessity for domain specific retraining.

Supporting this approach, we introduce CSeg, a new dataset tailored explicitly for the prompt conditioned change detection tasks involving unaligned imagery. CSeg employs advanced inpainting techniques to simulate realistic change scenarios, significantly reducing the manual labeling effort typically required. The dataset also incorporates intentional “red herring” changes, preventing the model from erroneously identifying inpainting artifacts as meaningful changes, thereby improving its generalization capability in real-world contexts.

Our extensive experiments illustrate that ViewDelta achieves competitive performance relative to specialized, domain-specific models trained exclusively on aligned images. These results hold consistently across varied settings, including indoor, outdoor, street-level, synthetic, and satellite imagery. Our contributions include:

- Introducing a novel text prompt conditioned change detection task that outputs binary segmentations based on user-specified textual descriptions of relevant changes.
- Proposing ViewDelta, the first transformer-based multi-modal architecture explicitly designed for prompt conditioned change detection.
- Creating and publicly releasing the CSeg dataset, comprising aligned and unaligned image pairs with corresponding textual prompts and annotated segmentation masks, facilitating future research.
- Demonstrating the first generalized change detection model capable of robustly performing across diverse image domains without retraining.

2. Related Work

Change Detection: Change detection (CD) entails identifying variations between two images, I_a and I_b , captured at different times and potentially from different viewpoints, producing a binary change map $M \in \{0, 1\}^{H \times W}$ that indicates altered regions. Traditional CD methods have largely focused on 2D image pairs with minimal or no viewpoint changes, as commonly seen in applications such as surveillance and satellite imagery [2, 16, 17, 51]. More recent approaches have extended CD to complex 3D settings, where the camera poses of I_a and I_b may vary significantly, and even to inherently 3D data like point clouds [1, 25, 34, 43]. This shift toward viewpoint variability introduces additional challenges, particularly in accurately annotating changes under varying viewpoints, which makes manual annotation costly and complex.

To address the difficulties associated with labeling under variable viewpoints, some methods leverage synthetic data or 3D representations. However, these advancements have been constrained by a lack of large-scale, real-image datasets annotated for CD with viewpoint variation. Consequently, models trained in these scenarios are often limited to synthetic data or rely on 3D modalities restricting the potential use cases to only scenarios where 3D data is available. This creates a need for real-image CD models robust enough to handle diverse viewpoints. To address this gap, we leverage three datasets. For the first dataset, we use the PSCD dataset [36] which consists of shifted panoramic images that, when cropped, shows slight variation in views. For the second dataset, we use the SYSU-CD [37] dataset which consists of fixed view satellite imagery. Finally to expand the models vocabulary and introduce more variation to view, we create CSeg, a dataset consisting of multi-view real images with multiple inpainted changes.

Semantic Change Detection: Unlike traditional CD, Semantic Change Detection consists of multiple categories of changes that must be selected similarly to semantic segmentation [12, 40, 46]. Given I_a and I_b , the objective of semantic change detection is to predict a semantic segmentation map $S \in \{1, 2, \dots, N\}^{H \times W}$, where N is the total number of semantic classes. Each pixel $S_{i,j}$ is assigned a class label $c \in \{1, 2, \dots, N\}$, identifying the type of semantic change corresponding to that region. Semantic change detection has been successfully applied to various types of imagery, including satellite [46], street view [36], and warehouse [31] images. However, current methods are typically tailored to specific domains, and a unified model that can generalize across different categories within a single saved checkpoint does not yet exist. With ViewDelta due to our unique formulation of CD with a text prompt, we are able to jointly train on multiple datasets and create a single saved model that achieve state of the art performance rather than a finetuned model for each dataset.

Open Vocabulary Image Segmentation: Open Vocabulary Image Segmentation is a computer vision task that involves labeling each pixel with categories beyond a predefined set, including categories potentially unseen during training [26, 27, 50]. This flexibility is achieved through models that associate text and image features, often utilizing vision-language frameworks like CLIP [32], which align visual and textual embeddings within a shared space. Our approach builds on these methods by integrating text and image models to enhance change detection. Rather than highlighting all possible changes, our model interprets a user-provided text prompt to selectively highlight changes relevant to the specified user text.

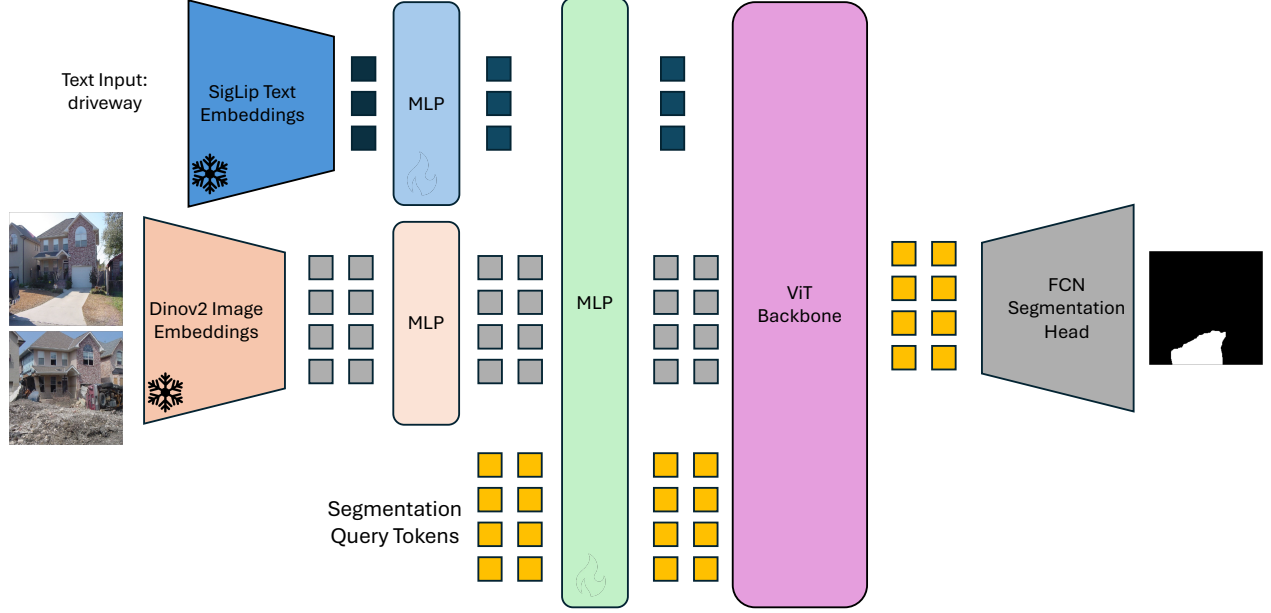


Figure 2. Overview diagram of the ViewDelta architecture consisting of two primary branches to process images and text. Both the text and image embedding network are frozen during training and never optimized. Text and image embeddings are concatenated with segmentation tokens before projection with an MLP before feeding into a ViT-Base backbone. Four layers of convolutions are applied with up sampling to decode the output features into a binary mask.

3. ViewDelta

In this section, we introduce **ViewDelta**, our proposed architecture for text-prompted change detection, as illustrated in Fig. 2. ViewDelta processes two input images, I_a and I_b , captured before and after a change event, respectively, along with a text prompt T that specifies the type of change relevant to the user. The goal is to predict a binary segmentation map $M \in \{0, 1\}^{H \times W}$, where $M_{i,j} = 1$ indicates the presence of the specified change at pixel location (i, j) and $M_{i,j} = 0$ otherwise.

The proposed architecture introduces several key modifications to the Vision Transformer (ViT) [13] to effectively integrate text prompts. These modifications include integrating a frozen text encoder to transform the text prompt T into a sequence of tokens, using an image encoder instead of a traditional patch embedding network for processing the input images I_a and I_b , introducing learned segmentation query tokens, and employing a fully convolutional segmentation head. The segmentation head specifically produces the final binary segmentation map M from the learned segmentation query tokens. These design choices primarily enable efficient training by leveraging pretrained networks, crucial given the limited number of training examples, while still exploiting the flexible but data-intensive transformer architecture.

3.1. Text Embeddings

We leverage only the text encoder of the SigLip [48] model due to its improved performance against models such as CLIP [32], OpenCLIP [15], and EVA-CLIP [42]. We leave the SigLip model frozen in order to keep the text generalization ability of SigLip. We evaluate the generalizability of the model on the CSeg dataset which contains unique prompts in the test set that are not seen in the training set.

3.2. Image Embeddings

Patch embeddings have been widely adopted by state-of-the-art methods in both change detection and semantic segmentation. However, in our joint training configuration, we observed that optimizing patch embeddings was challenging due to the slow convergence rate on the available training data. To address this issue, we investigated directly using image features from a frozen Dinov2 [29] model as embeddings. Our ablation study shall demonstrate that Dinov2 embeddings yielded faster convergence rate with less data. We attribute the difficulty of optimizing learned patch embeddings primarily to dataset size limitations rather than inherent issues with patch embeddings themselves. Scaling the model and dataset could further improve performance but would require significantly increased computational resources and data availability, as such this will be investigated further in follow up works that will scale our dataset and model size.

3.3. Backbone

We utilize the ViT [13] transformer architecture in its base configuration as the backbone, consisting of 12 transformer encoder layers, each characterized by a hidden dimension of 768, an intermediate MLP dimension of 3072, and 12 attention heads. Diverging from typical approaches, this backbone abstains from assumptions regarding spatial alignment and refrains from explicit feature aggregation strategies, such as subtraction or concatenation, commonly employed in models like FC-EF [11], STANet [8], [7], and DSAMNet [37]. Consequently, it achieves a generalized and robust multimodal representation without relying on a built-in bias for aligned images.

3.4. Segmentation Query Tokens

Drawing inspiration from DETR [5], we leverage dedicated segmentation query tokens to enhance model flexibility. These tokens facilitate the model to create streamlined representations for segmentation-related features, circumventing the inherent complexities encountered if the model had to directly map and align combined image and textual tokens to a feature space that could be used for change detection. This methodological choice effectively addresses issues of adding padding tokens or deciding which tokens from the sequence of image and text tokens to use as input into a segmentation head. State-of-the-art change detection methods that use transformers are able to circumvent this because images are aligned and text tokens are not incorporated.

3.5. Segmentation Head

Existing state-of-the-art change detection architectures, including SwinSUNet [49], ChangeFormerV4 [4], and MambaBCD-Base [7], predominantly assume spatial alignment between input image pairs, inherently limiting their applicability in practical scenarios involving unaligned or varying viewpoints. To overcome this limitation, we adopt a segmentation that exclusively operates only on segmentation query tokens, as shown in Algorithm 1. This design choice removes the necessity of explicit feature combination from spatially mismatched input images and facilitates effective fusion of visual and textual embeddings. The implemented segmentation head comprises of a concise structure of four convolutional layers followed by upsampling, forming a robust yet straightforward framework for investigating performance and generalization in text-conditioned change detection.

Algorithm 1 Forward prediction of proposed model

Require: Images I_a, I_b and text embeddings T_e

- 1: $I_a \leftarrow \text{ImageEmbedder}(I_a)$
- 2: $I_b \leftarrow \text{ImageEmbedder}(I_b)$
- 3: $T \leftarrow \text{TextEmbedder}(T_e)$
- 4: $X \leftarrow \text{Concat}(I_a, I_b, T, \text{SegEmbeddings})$
- 5: $X \leftarrow X + \text{PositionalEmbedding}$
- 6: $X \leftarrow \text{MLP}(X)$
- 7: $X \leftarrow \text{ViT}(X)$
- 8: $\text{SegEmbeddings} \leftarrow X[:, -N_s :, :]$
- 9: $\text{SegLogits} \leftarrow \text{UpsampleNetwork}(\text{SegEmbeddings})$
- 10: **return** SegLogits

3.6. Implementation Details

PSCD view variation: The PSCD dataset comprises of 770 panoramic image pairs captured in a suburban environment. Though the PSCD dataset was originally released for view aligned change detection of panoramic images, from further inspection, we have found that, when zoomed in, the dataset was found to have some varying amounts of view-point change. To leverage this data as a source of real street level change detection we take each panoramic image and extract non-overlapping crops of size 256×256 . The labels provided by PSCD are originally intended for semantic segmentation across classes such as vehicles and people. We use these classes to generate several binary segmentation masks, with each class serving as a distinct text prompt for segmentation.

Training Details: ViewDelta is jointly trained across multiple datasets using the Adam optimizer [21] with weight decay, a one-epoch warm-up, and cosine annealing learning rate decay, starting from an initial learning rate of 2×10^{-5} . Training is performed using a batch size of 4 per GPU using 4 Nvidia A100 GPUs, resulting in an effective batch size of 16. We utilize DeepSpeed ZeRO Stage 2 [33] for sharding optimizer states and gradients, activation checkpointing within attention layers and large linear layer, and 16-bit mixed-precision training.

4. CSeg Dataset

A major factor contributing to recent advancements in deep learning is the accessibility of large-scale datasets with high-quality annotations. To the best of our knowledge, there is currently no existing dataset that contains image pairs with text-guided change masks, especially those that involve view shifts. Although the processed PSCD dataset provides minor view alignment differences, it is limited to traffic-like classes such as “vehicles”, “barrier”, “human”, and “lane marking”. A dataset that addresses these issues will significantly accelerate progress in the change detection field. However, manually labeling thousands of image pairs with changes is cumbersome, expensive, and imprac-

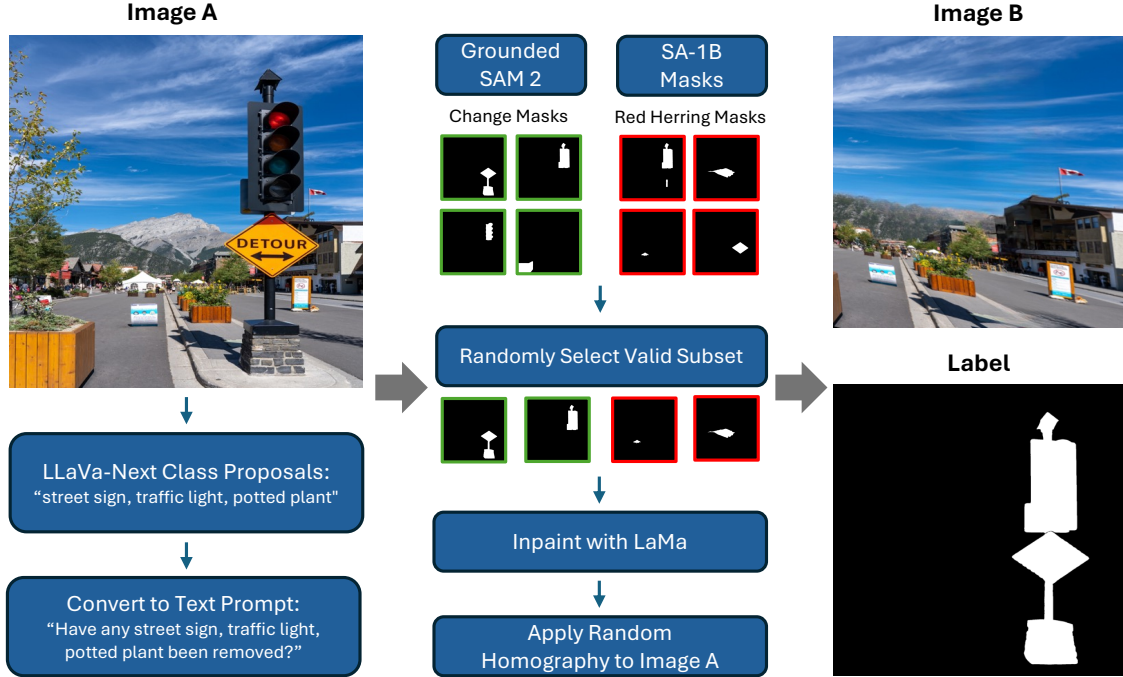


Figure 3. Overview of CSeg generation. We select an SA-1B image and leverage LLaVa-Next to propose multiple class proposals that exist in the image. These classes are then converted to a natural language change prompt and also are fed into Grounded SAM 2 to collect instance masks on all class proposals. These masks are collected and inpainted to simulate change while the SA-1B provided masks are used as red herring masks. This results in a text prompt, image A, image B, and change mask label.

tical to scale. Inspired by the COCO-Inpainted dataset [34], we propose a procedure that leverages state of the art vision models to generate the Change Segmentation (CSeg) dataset: a large-scale, varying-view, and text-guided change detection dataset.

4.1. Inpainting Changes

Instead of manually creating and labeling change images, we employ inpainting to synthetically simulate changes between two images. To achieve this, we first select an SA-1B [22] image and leverage LLaVa-Next [24] to identify a maximum of ten different objects in the image to be used as classes. To promote dataset balance, we select one to five of the least represented classes during generation. These classes are then used directly as text prompts or applied to a natural language prompt template. These prompt templates are a list of 45 predefined and manually validated templates generated with GPT-4o that have the intent of identifying change. To simulate change, Grounded SAM 2 is then used to generate instance masks across classes, and we randomly select a subset of at most 10 masks to be inpainted in image B with LaMa [44]. We combine these inpainted masks to produce the change label. Finally, we apply a random homography change to either image A or image B to simulate a perspective change.

ViewDelta should be generalized to detect all changes in an image and not limited to those specified by a prompt which eliminates the need for explicit class enumeration. To generate these “all” image pairs, we randomly inpaint five to ten SA-1B masks on image B to simulate change. The text prompt is randomly selected from a predefined list of 96 prompts generated with GPT-4o that convey an intent for all changes.

4.2. Combating Inpainting Noise

Although inpainting produces seemingly realistic changes, we noticed that the inpainted regions tend to have inpainting artifacts (as observed in other works in the literature [9, 10, 19]). We use “red herring” masks to prevent the model from learning artifacts instead of image changes. These red herring masks are a randomly selected subset of zero to ten SA-1B masks that are not classified as any of the classes in the text prompt. Since SA-1B doesn’t provide mask classifications, we use Grounded SAM 2 with a low confidence threshold to ensure that the SA-1B mask doesn’t coincide with a change class instance. These red herring masks are inpainted on image B but not added to the change mask. During training, this forces the model to learn the change between the two images that are consistent with text prompt rather than labeling inpainting noise

as changes. Adding red herring masks to “all” image pairs is not applicable, since every change needs to be accounted for which would include all inpaints.

4.3. Dataset Statistics

There is a total of 501,153 change image pairs in CSeg split into 451,090 pairs in train and 50,063 in test. There are 24,298 unique classes and 339,348 unique prompts in train and 7,285 unique classes and 7,326 unique prompts in test. There are 1,408 unique classes and 35,271 unique prompts not seen in train. 53,257 and 5,947 pairs were “all” image pairs in the train and test sets respectively at about a 12% of the total for each set. CSeg’s class counts are top heavy in that more common classes such as “clouds”, “sky”, “people”, “water”, “trees” and “roof” appear exponentially more often than less common classes like “calcite”, “aldravanda”, and “ice hammer” as depicted in Fig. 4. This is due to how the majority of images in SA-1B include these common objects. During class proposals, we select the classes that are least used in CSeg to mitigate this problem.

Although LLaVa-Next and Grounded SAM 2 are very impressive vision models, they cannot produce flawless class proposals and instance masks for all images. This consequently affects the quality of CSeg. To quantitatively measure the quality of CSeg, we manually check randomly sampled images until the percent accuracy clearly converges. We validated 500 images - about 0.1% of the entire dataset - and observed an accuracy of 94.0%. This results in a margin of error of $\pm 2.22\%$ at a 95% statistical confidence. The large majority of errors stem from Grounded SAM 2 yielding masks that are misclassified, especially with more challenging classes. We provide additional examples in Fig. 5 for further evaluation.

5. Experiments

To assess the effectiveness of ViewDelta, we evaluate its performance on three diverse datasets: CSeg, PSCD [36], and SYSU-CD [37]. These datasets cover a broad range of domains, including indoor, outdoor, street-view, and satellite imagery, ensuring a comprehensive evaluation across different contexts.

This section first presents quantitative metrics for each dataset, evaluating several state-of-the-art models on each dataset individually and reporting metrics such as intersection over union (IoU). Following this, we provide a qualitative analysis, showcasing examples of ViewDelta’s performance across various samples in the dataset.

5.1. Quantitative Evaluation

We quantitatively evaluate the performance of ViewDelta on three diverse datasets: CSeg, PSCD [36], and SYSU-CD [37], comparing it against several state-of-the-art methods using standard metrics, including Intersection over Union

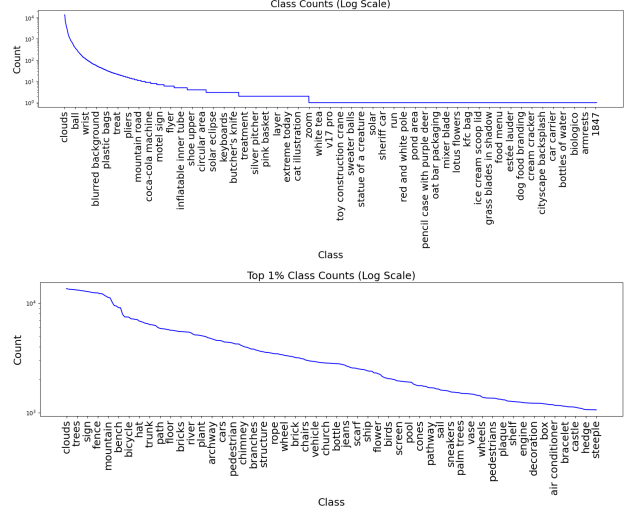


Figure 4. Class count distributions: top 1% most frequent classes and the complete dataset. These figures don’t include the “all” class. As class counts decrease, the class gets more impractical.

Model	IoU	F1	Rec	Prec
ViewDelta	85.91	92.42	89.25	95.82

Table 1. Quantitative Results On The CSeg Dataset by a jointly trained model, the checkpoint used is the same across all reported results for the general model. The CSeg test set contains prompts not seen in the training set.

Model	IoU	F1	Rec	Prec
<i>Fine-tuned models</i>				
CSCDNet	22.3	—	—	—
+ SSCDNet [36]	32.2	—	—	—
CSSCDNet [36]	32.2	—	—	—
ViewDelta	55.54	78.31	69.47	73.47
<i>General model</i>				
ViewDelta	52.24	68.63	72.57	65.10

Table 2. Quantitative Results on PSCD Dataset. The highest values are highlighted in bold and the general model results are from the same checkpoint across all results.

(IoU), F1 score, Recall (Rec), and Precision (Prec). Results are summarized in Tabs. 1 to 3.

On the CSeg dataset Tab. 1, ViewDelta achieves excellent performance, with an IoU of 85.91%, an F1 score of 92.42%, a recall of 89.25%, and notably high precision of 95.82%.

For the PSCD dataset Tab. 2, which includes view-point changes and challenging illumination conditions,

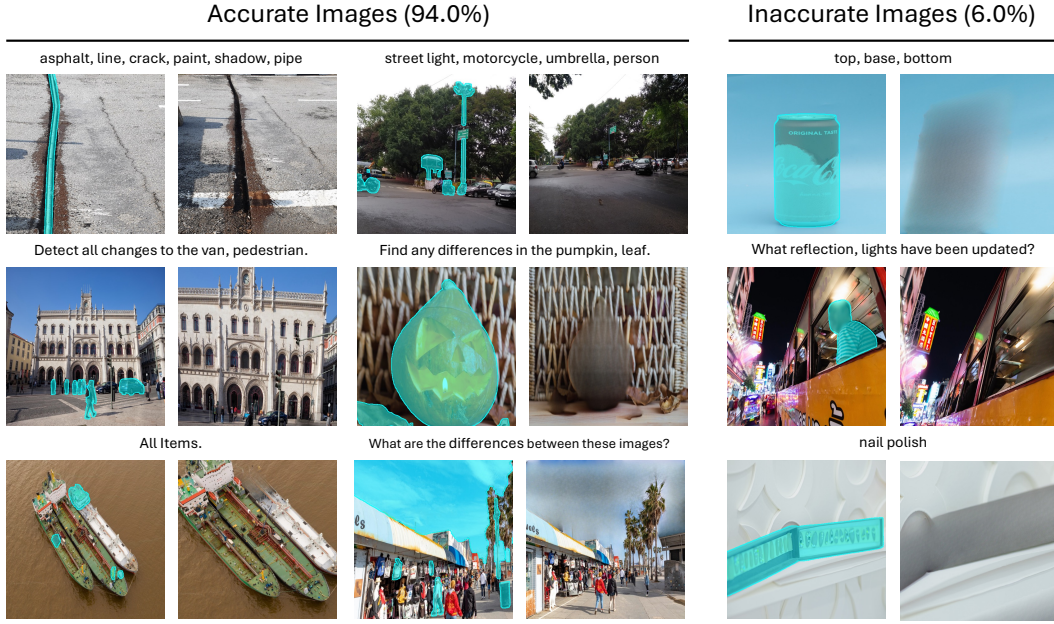


Figure 5. Evaluation of CSeg quality. Change mask label is highlighted in blue. Manual inspection of the generated images show a 94% agreement with a human reviewer.



Figure 6. **Qualitative Results:** We show ViewDelta predictions in red on the test sets, along with the ground truth in blue. All SYSU-CD test images use the text prompt of: “urban development, suburban expansion, pre-construction groundwork, vegetation alteration, road widening, and coastal construction”.

Method	IoU	F1	Rec	Prec
<i>Fine-tuned models</i>				
FC-EF [11]	61.04	75.81	75.17	76.47
FC-Siam-diff [11]	61.01	75.79	75.30	76.28
FC-Siam-conc [11]	60.23	75.18	76.75	73.67
BiDateNet [30]	62.52	76.94	72.60	81.84
STANet [8]	63.09	77.37	85.33	70.76
DSAMNet [37]	64.18	78.18	81.86	74.81
ChangeFormerV4 [4]	65.03	78.81	77.90	79.74
BIT-50 [6]	66.14	79.62	77.90	81.42
TransUNetCD [23]	66.79	80.09	77.73	82.59
SwinUNet [49]	68.89	81.58	79.75	83.50
MambaBCD [7]	71.10	83.11	80.31	86.11
ViewDelta	70.09	82.41	79.91	85.08
<i>General model</i>				
ViewDelta	68.59	81.37	75.42	88.33

Table 3. Quantitative Results on SYSU-CD Dataset. The highest values are highlighted for **First** and **Second**. The general model results are from the same checkpoint across all results. We additionally finetune the general ViewDelta model to evaluate its fine-tuning performance.

ViewDelta significantly outperforms prior fine-tuned methods, achieving an IoU of 55.54%, an F1 score of 78.31%, recall of 69.47%, and precision of 73.47%. The general model also shows strong performance with an IoU of 52.24%.

Finally, on the SYSU-CD dataset Tab. 3, consisting of satellite imagery, the ViewDelta fine-tuned model achieves competitive results with an IoU of 70.09% and an F1 score of 82.41%, closely following the state-of-the-art MambaBCD-Base method. The general model maintains strong performance, achieving an IoU of 68.59% and demonstrating superior precision at 88.33%.

These results demonstrate competitive performance across datasets, underscoring ViewDelta’s robustness. We attribute this success to the model’s multi-domain training approach. Given this strong performance from a relatively simple architecture, we anticipate that further architectural enhancements or specialized fine-tuning approaches could lead to even more substantial performance improvements in the future.

5.2. Qualitative Evaluation

We present qualitative results of our model on example image pairs from the CSeg, PSCD, and SYSU-CD test sets in Fig. 6. For the SYSU-CD test set, all images use the text prompt: “urban development, suburban expansion, pre-construction groundwork, vegetation alteration, road widening, and coastal construction.” For the PSCD test set, each image uses a prompt corresponding to the classes de-

fined in the dataset, such as “vehicle” or “structure.”

5.3. Ablation Study

We perform extensive ablation studies to investigate the impact of various embedding strategies on the training efficiency of ViewDelta. First, we evaluate combinations of image and text embeddings on a random subset of the CSeg dataset containing 22,624 images, allowing models to train for 12 hours. Results are presented in Tab. 4.

Embeddings	IoU
SigLip + Dinov2	56.44
SigLip + Patch Embedding	26.16
CLIP + Dinov2	53.46
CLIP + Patch Embedding	27.56

Table 4. Evaluation of embedding combinations on a subset of CSeg.

The results demonstrate that the combination of SigLip text embeddings and Dinov2 image embeddings consistently outperforms other configurations. Additionally, using Dinov2 embeddings significantly surpasses patch embeddings, regardless of text encoder choice.

Further, we evaluate the specific impact of frozen Dinov2 embeddings compared to fully-trained patch embeddings across multiple datasets simultaneously. Both configurations use SigLip for text embeddings, and results are summarized in Tab. 5.

Image Embedding	CSeg	PSCD	SYSU-CD
Frozen Dinov2	85.91	52.24	68.59
Patch Embedding	61.05	16.87	34.81

Table 5. Impact of frozen Dinov2 versus trained patch embeddings across multiple datasets.

We observe that frozen Dinov2 embeddings significantly outperform fully-trained patch embeddings, indicating that pretrained image embeddings not only provide a more robust feature representation but also improve convergence speed and overall model generalization. This advantage is particularly pronounced given the dataset size limitations encountered in our training scenarios.

5.4. Limitations

CSeg is limited to synthetic perspective differences, which limits the models generalizability to large perspective changes. Expanding the dataset to include larger perspective changes is challenging due to the limited availability of the required data in addition to the difficulty in labeling the data. Lack of real data of image pairs with textual prompts.

Another limitation is the exponential increase in the number of image tokens required for higher resolution images that may contain small changes. However, this can be mitigated as compute is scaled.

6. Conclusion

We presented ViewDelta, a novel multimodal architecture for text-prompted change detection capable of processing unaligned images through the integration of natural language prompts. By leveraging pretrained text and image embeddings, ViewDelta effectively generalizes across diverse domains without requiring retraining for novel changes. We introduced the CSeg dataset, a comprehensive dataset specifically crafted for text-conditioned change detection tasks, providing over 500,000 image pairs with associated textual prompts and annotated binary masks. Extensive experiments demonstrated that ViewDelta achieves robust and competitive performance across various challenging domains, including indoor, outdoor, street-level, synthetic, and satellite imagery. Our findings underscore the model’s flexibility and effectiveness, paving the way for future advancements in generalized, text-conditioned change detection methodologies.

References

- [1] Aikaterini Adam, Konstantinos Karantzas, Lazaros Grammatikopoulos, and Torsten Sattler. Has anything changed? 3d change detection by 2d segmentation masks, 2023. 2
- [2] Abdulaziz Amer Aleissae, Amandeep Kumar, Rao Muhammad Anwer, Salman Khan, Hisham Cholakkal, Gui-Song Xia, and Fahad Shahbaz Khan. Transformers in remote sensing: A survey. *Remote Sensing*, 15(7):1860, 2023. 2
- [3] Ting Bai, Le Wang, Dameng Yin, Kaimin Sun, Yepi Chen, Wenzhuo Li, and Deren Li. Deep learning for change detection in remote sensing: a review. *Geo-spatial Information Science*, 26(3):262–288, 2023. 1
- [4] Wele Gedara Chaminda Bandara and Vishal M Patel. A transformer-based siamese network for change detection. In *IGARSS 2022-2022 IEEE International Geoscience and Remote Sensing Symposium*, pages 207–210. IEEE, 2022. 4, 8
- [5] Nicolas Carion, Francisco Massa, Gabriel Synnaeve, Nicolas Usunier, Alexander Kirillov, and Sergey Zagoruyko. End-to-end object detection with transformers, 2020. 4
- [6] Hao Chen, Zipeng Qi, and Zhenwei Shi. Remote sensing image change detection with transformers. *IEEE Transactions on Geoscience and Remote Sensing*, 60:1–14, 2021. 8
- [7] Hongruixuan Chen, Jian Song, Chengxi Han, Junshi Xia, and Naoto Yokoya. Changemamba: Remote sensing change detection with spatio-temporal state space model. *IEEE Transactions on Geoscience and Remote Sensing*, 2024. 4, 8
- [8] Gong Cheng, Ceyuan Yang, Xiwen Yao, Lei Guo, and Junwei Han. When deep learning meets metric learning: Remote sensing image scene classification via learning discriminative cnns. *IEEE Transactions on Geoscience and Remote Sensing*, 56:2811–2821, 2018. 4, 8
- [9] Guangliang Cheng, Yunmeng Huang, Xiangtai Li, Shuchang Lyu, Zhaoyang Xu, Hongbo Zhao, Qi Zhao, and Shiming Xiang. Change detection methods for remote sensing in the last decade: A comprehensive review. *Remote Sensing*, 16(13):2355, 2024. 1, 5
- [10] Antonio Criminisi, Patrick Pérez, and Kentaro Toyama. Region filling and object removal by exemplar-based image inpainting. *IEEE Transactions on image processing*, 13(9):1200–1212, 2004. 5
- [11] Rodrigo Caye Daudt, Bertrand Le Saux, and Alexandre Boulch. Fully convolutional siamese networks for change detection, 2018. 4, 8
- [12] Lei Ding, Haitao Guo, Sicong Liu, Lichao Mou, Jing Zhang, and Lorenzo Bruzzone. Bi-temporal semantic reasoning for the semantic change detection in hr remote sensing images. *IEEE Transactions on Geoscience and Remote Sensing*, 60:1–14, 2022. 2
- [13] Alexey Dosovitskiy, Lucas Beyer, Alexander Kolesnikov, Dirk Weissenborn, Xiaohua Zhai, Thomas Unterthiner, Mostafa Dehghani, Matthias Minderer, Georg Heigold, Sylvain Gelly, Jakob Uszkoreit, and Neil Houlsby. An image is worth 16x16 words: Transformers for image recognition at scale. *CoRR*, abs/2010.11929, 2020. 3, 4
- [14] Zhihang Fu, Yaowu Chen, Hongwei Yong, Rongxin Jiang, Lei Zhang, and Xian-Sheng Hua. Foreground gating and background refining network for surveillance object detection. *IEEE Transactions on Image Processing*, PP:1–1, 2019. 1
- [15] Samir Yitzhak Gadre, Gabriel Ilharco, Alex Fang, Jonathan Hayase, Georgios Smyrnis, Thao Nguyen, Ryan Marten, Mitchell Wortsman, Dhruva Ghosh, Jieyu Zhang, et al. Datcomp: In search of the next generation of multimodal datasets. *Advances in Neural Information Processing Systems*, 36, 2024. 3
- [16] Andrew Gonzalez, Jonathan M Chase, and Mary I O’Connor. A framework for the detection and attribution of biodiversity change. *Philosophical Transactions of the Royal Society B*, 378(1881):20220182, 2023. 2
- [17] Ebrahim Hamidi, Brad G Peter, David F Muñoz, Hamed Moftakhari, and Hamid Moradkhani. Fast flood extent monitoring with sar change detection using google earth engine. *IEEE Transactions on Geoscience and Remote Sensing*, 61:1–19, 2023. 2
- [18] Ji Han, Xing Meng, Xiang Zhou, Bailu Yi, Min Liu, and Wei-Ning Xiang. A long-term analysis of urbanization process, landscape change, and carbon sources and sinks: A case study in china’s yangtze river delta region. *Journal of Cleaner Production*, 141:1040–1050, 2017. 1
- [19] Jiaya Jia and Chi-Keung Tang. Image repairing: Robust image synthesis by adaptive nd tensor voting. In *2003 IEEE Computer Society Conference on Computer Vision and Pattern Recognition, 2003. Proceedings.*, pages I–I. IEEE, 2003. 5
- [20] Huiwei Jiang, Min Peng, Yuanjun Zhong, Haofeng Xie, Zemin Hao, Jingming Lin, Xiaoli Ma, and Xiangyun Hu. A

- survey on deep learning-based change detection from high-resolution remote sensing images. *Remote Sensing*, 14(7): 1552, 2022. 1
- [21] Diederik P Kingma. Adam: A method for stochastic optimization. *arXiv preprint arXiv:1412.6980*, 2014. 4
- [22] Alexander Kirillov, Eric Mintun, Nikhila Ravi, Hanzi Mao, Chloe Rolland, Laura Gustafson, Tete Xiao, Spencer Whitehead, Alexander C Berg, Wan-Yen Lo, et al. Segment anything. In *Proceedings of the IEEE/CVF international conference on computer vision*, pages 4015–4026, 2023. 5
- [23] Qingyang Li, Ruofei Zhong, Xin Du, and Yu Du. Transunetcd: A hybrid transformer network for change detection in optical remote-sensing images. *IEEE Transactions on Geoscience and Remote Sensing*, 60:1–19, 2022. 8
- [24] Haotian Liu, Chunyuan Li, Yuheng Li, Bo Li, Yuanhan Zhang, Sheng Shen, and Yong Jae Lee. Llava-next: Improved reasoning, ocr, and world knowledge, 2024. 5
- [25] Ziqi Lu, Jianbo Ye, and John Leonard. 3dgs-cd: 3d gaussian splatting-based change detection for physical object re-arrangement, 2024. 2
- [26] Timo Lüddecke and Alexander Ecker. Image segmentation using text and image prompts. In *Proceedings of the IEEE/CVF conference on computer vision and pattern recognition*, pages 7086–7096, 2022. 2
- [27] Huaishao Luo, Junwei Bao, Youzheng Wu, Xiaodong He, and Tianrui Li. Segclip: Patch aggregation with learnable centers for open-vocabulary semantic segmentation. In *International Conference on Machine Learning*, pages 23033–23044. PMLR, 2023. 2
- [28] Tim Newbold, Lawrence N Hudson, Samantha LL Hill, Sara Contu, Igor Lysenko, Rebecca A Senior, Luca Börger, Dominic J Bennett, Argyrios Choimes, Ben Collen, et al. Global effects of land use on local terrestrial biodiversity. *Nature*, 520(7545):45–50, 2015. 1
- [29] Maxime Oquab, Timothée Darcet, Théo Moutakanni, Huy Vo, Marc Szafraniec, Vasil Khalidov, Pierre Fernandez, Daniel Haziza, Francisco Massa, Alaaeldin El-Nouby, Mahmoud Assran, Nicolas Ballas, Wojciech Galuba, Russell Howes, Po-Yao Huang, Shang-Wen Li, Ishan Misra, Michael Rabbat, Vasu Sharma, Gabriel Synnaeve, Hu Xu, Hervé Jegou, Julien Mairal, Patrick Labatut, Armand Joulin, and Piotr Bojanowski. Dinov2: Learning robust visual features without supervision, 2024. 3
- [30] Maria Papadomanolaki, Sagar Verma, Maria Vakalopoulou, Siddharth Gupta, and Konstantinos Karantzas. Detecting urban changes with recurrent neural networks from multi-temporal sentinel-2 data, 2019. 8
- [31] Jin-Man Park, Jae-hyuk Jang, Sahng-Min Yoo, Sun-Kyung Lee, Ue-hwan Kim, and Jong-Hwan Kim. Changesim: Towards end-to-end online scene change detection in industrial indoor environments. In *2021 IEEE/RSJ International Conference on Intelligent Robots and Systems (IROS)*. IEEE, 2021. 2
- [32] Alec Radford, Jong Wook Kim, Chris Hallacy, Aditya Ramesh, Gabriel Goh, Sandhini Agarwal, Girish Sastry, Amanda Askell, Pamela Mishkin, Jack Clark, et al. Learning transferable visual models from natural language supervision. In *International conference on machine learning*, pages 8748–8763. PMLR, 2021. 2, 3
- [33] Samyam Rajbhandari, Jeff Rasley, Olatunji Ruwase, and Yuxiong He. Zero: Memory optimizations toward training trillion parameter models. In *SC20: International Conference for High Performance Computing, Networking, Storage and Analysis*, pages 1–16. IEEE, 2020. 4
- [34] Ragav Sachdeva and Andrew Zisserman. The change you want to see (now in 3d). In *Proceedings of the IEEE/CVF International Conference on Computer Vision*, pages 2060–2069, 2023. 2, 5
- [35] Keiko Saito, Robin JS Spence, Christopher Going, and Michael Markus. Using high-resolution satellite images for post-earthquake building damage assessment: a study following the 26 january 2001 gujarat earthquake. *Earthquake spectra*, 20(1):145–169, 2004. 1
- [36] Ken Sakurada, Mikiya Shibuya, and Weimin Wang. Weakly supervised silhouette-based semantic scene change detection, 2022. 2, 6
- [37] Qian Shi, Mengxi Liu, Shengchen Li, Xiaoping Liu, Fei Wang, and Liangpei Zhang. A deeply supervised attention metric-based network and an open aerial image dataset for remote sensing change detection. *IEEE Transactions on Geoscience and Remote Sensing*, pages 1–16, 2021. 2, 4, 6, 8
- [38] Wenzhong Shi, Min Zhang, Rui Zhang, Shanxiong Chen, and Zhao Zhan. Change detection based on artificial intelligence: State-of-the-art and challenges. *Remote Sensing*, 12(10):1688, 2020. 1
- [39] Ashbindu Singh. Review article digital change detection techniques using remotely-sensed data. *International journal of remote sensing*, 10(6):989–1003, 1989. 1
- [40] Jian Song, Hongruixuan Chen, and Naoto Yokoya. Syntheworld: A large-scale synthetic dataset for land cover mapping and building change detection. In *Proceedings of the IEEE/CVF Winter Conference on Applications of Computer Vision (WACV)*, pages 8287–8296, 2024. 2
- [41] Jérémie Sublime and Ekaterina Kalinicheva. Automatic post-disaster damage mapping using deep-learning techniques for change detection: Case study of the tohoku tsunami. *Remote Sensing*, 11(9):1123, 2019. 1
- [42] Quan Sun, Yuxin Fang, Ledell Wu, Xinlong Wang, and Yue Cao. Eva-clip: Improved training techniques for clip at scale. *arXiv preprint arXiv:2303.15389*, 2023. 3
- [43] Yanjun Sun, Yue Qiu, Mariia Khan, Fumiya Matsuzawa, and Kenji Iwata. The stvchron dataset: Towards continuous change recognition in time. In *Proceedings of the IEEE/CVF Conference on Computer Vision and Pattern Recognition (CVPR)*, pages 14111–14120, 2024. 2
- [44] Roman Suvorov, Elizaveta Logacheva, Anton Mashikhin, Anastasia Remizova, Arsenii Ashukha, Aleksei Silvestrov, Naejin Kong, Harshith Goka, Kiwoong Park, and Victor Lempitsky. Resolution-robust large mask inpainting with fourier convolutions. *arXiv preprint arXiv:2109.07161*, 2021. 5
- [45] Chuyi Wu, Feng Zhang, Junshi Xia, Yichen Xu, Guoqing Li, Jibo Xie, Zhenhong Du, and Renyi Liu. Building damage

- detection using u-net with attention mechanism from pre-and post-disaster remote sensing datasets. *Remote Sensing*, 13(5):905, 2021. [1](#)
- [46] Kunping Yang, Gui-Song Xia, Zicheng Liu, Bo Du, Wen Yang, Marcello Pelillo, and Liangpei Zhang. Semantic change detection with asymmetric siamese networks, 2021. [2](#)
- [47] Shuai Yi, Hongsheng Li, and Xiaogang Wang. Pedestrian behavior modeling from stationary crowds with applications to intelligent surveillance. *Trans. Img. Proc.*, 25(9):4354–4368, 2016. [1](#)
- [48] Xiaohua Zhai, Basil Mustafa, Alexander Kolesnikov, and Lucas Beyer. Sigmoid loss for language image pre-training. In *Proceedings of the IEEE/CVF International Conference on Computer Vision*, pages 11975–11986, 2023. [3](#)
- [49] Cui Zhang, Liejun Wang, Shuli Cheng, and Yongming Li. Swinsunet: Pure transformer network for remote sensing image change detection. *IEEE Transactions on Geoscience and Remote Sensing*, 60:1–13, 2022. [4](#), [8](#)
- [50] Hang Zhao, Xavier Puig, Bolei Zhou, Sanja Fidler, and Antonio Torralba. Open vocabulary scene parsing. In *Proceedings of the IEEE International Conference on Computer Vision*, pages 2002–2010, 2017. [2](#)
- [51] Qiqi Zhu, Xi Guo, Ziqi Li, and Deren Li. A review of multi-class change detection for satellite remote sensing imagery. *Geo-spatial Information Science*, 27(1):1–15, 2024. [2](#)